PERGAMON

International Journal of Heat and Mass Transfer 45 (2002) 993–1006

International Journal of HEAT and MASS TRANSFER

www.elsevier.com/locate/ijhmt

Heat transfer characteristics of a slot jet impinging on a semi-circular convex surface

T.L. Chan [a,*], C.W. Leung [a], K. Jambunathan [b], S. Ashforth-Frost [b], Y. Zhou [a], M.H. Liu [a]

[a] *Department of Mechanical Engineering, The Hong Kong Polytechnic University, Hung Hom, Kowloon, Hong Kong*
[b] *Department of Mechanical and Manufacturing Engineering, The Nottingham Trent University, Nottingham NG1 4BU, UK*

Received 18 February 2001; received in revised form 30 June 2001

Abstract

Surface heat transfer characteristics of a heated slot jet impinging on a semi-circular convex surface have been investigated by using the transient heating liquid crystal technique. Free jet velocity, turbulence and temperature characteristics have been determined by using a combination of an X-wire and a cold wire anemometry. The parametric effects of jet Reynolds number (Re_W) ranging from 5600 to 13,200 and the dimensionless slot nozzle-to-impingement surface distance (Y/W) ranges from 2 to 10 on the local circumferential heat transfer have been studied. Local circumferential Nusselt number (Nu_S) decreases with increasing the dimensionless circumferential distance (S/W) from its maximum value at the stagnation point up to $S/W = 3.1$. The transition in the wall jet from laminar to turbulent flow was completed by about $3.3 \leqslant S/W \leqslant 4.2$ which coincided with a secondary peak in heat transfer. Correlations of local and average Nusselt numbers with Re_W, Y/W and S/W have been established for the stagnation point and the circumferential distribution. The rate of decay of average circumferential Nusselt numbers around the semi-circular convex surface is much faster than that which occurs laterally along the flat surface. As Y/W increases, the effect of surface curvature becomes apparent and the difference between the flat surface correlation and the convex surface becomes more pronounced.

Keywords: Jet impingement heat transfer; Surface curvature; Liquid crystal thermographic technique; Transient heating liquid crystal method

1. Introduction

Jet impingement heat transfer on a curved surface is commonly encountered in many engineering applications and manufacturing processes because of its high local heat transfer rates for heating, cooling, or drying a surface, and its low cost and simple control. Many industrial curved surface applications include, for example, the heating, cooling and/or drying of painted cylinders, glass, paper, textiles, film material, foodstuffs, age hardening, the de-icing of aircraft wings and safety requirements in the storage of cylinders containing liquefied gas. The optimization of such applications is becoming necessary as industry demands increased efficiency and safety.

A large number of publications on the case of simple geometries such as a confined/unconfined circular/slot jet impinging on a flat surface exist in the archived literature. It is because the fluid dynamic structure of such processes is extremely complex and, as such, the problem is often reduced to a single impinging jet which might be in laminar/turbulent flow. A number of critical reviews and bibliographical works on various aspects of the experimental, analytical and numerical work of flow and heat transfer characteristics under impinging jet(s)

* Corresponding author. Tel.: +852-2766-6656; fax: +852-2365-4703.
E-mail address: mmtlchan@polyu.edu.hk (T.L. Chan).

0017-9310/02/$ - see front matter
PII: S0017-9310(01)00217-4

Nomenclature

a, b, c, e, f, g, i, j	constant coefficients in Eqs. (5) and (6)
k, l, m, n, p, q	constant coefficients in Eqs. (10) and (11)
CCD	charge-coupled device
c_s	specific heat capacity of acrylic specimen
d	circular nozzle diameter
D	diameter of impingement cylinder
erf	Gaussian error function
h	local heat transfer coefficient
k_a	thermal conductivity of air
k_s	thermal conductivity of acrylic specimen
Nu_S	local Nusselt number in circumferential distance ($= hW/k_a$)
Nu_{ave}	averaged Nusselt number
Nu_0	stagnation Nusselt number
PAL	phase alternation line
r	overheat ratio, $(R_W - R_0)/R_0$
R	radius of a semi-circular convex surface
R_W	work resistance
R_0	calibration resistance
R30C5W	red start 30 °C, blue start 35 °C; the other colors exhibit between these 5 °C bandwidths
R35C5W	red start 35 °C, blue start 40 °C; the other colors exhibit between these 5 °C bandwidths
Re_d	Reynolds number of circular jet diameter at nozzle exit ($= U_j d/v$)
Re_W	Reynolds number of slot jet width at nozzle exit ($= U_j W/v$)
s	thickness of acrylic specimen
S	circumferential distance around a semi-circular convex surface from the centerline of the slot jet
t	time
T, A, H	temperature, viewing/illumination angle from the normal position and hue
T	local surface temperature
T_{amb}	initial wall (ambient) temperature
T_c	streamwise mean temperature along the centerline of a free slot jet
T_j	mean temperature at the slot jet exit
T_s	temperature of the environment surrounding the jet
$T_{(0,t)}$	local wall temperature at specific time
u, v	fluctuating velocities in x and y directions
U, V	mean velocities in x and y directions
U_c	streamwise mean velocity along the centerline of a free slot jet
U_j	mean velocity at the slot jet exit
W	slot nozzle width
X	lateral distance along the flat surface from the centerline of a slot jet
x, y	spatial coordinate system
Y	slot/circular jet-to-impingement surface distance
Greek symbols	
ϕ	normalized temperature in Eq. (2)
Θ	local mean temperature difference, $T_c - T_s$
Θ_j	maximum mean temperature difference, $T_j - T_s$
α_s	thermal diffusivity of acrylic specimen ($= k_s/\rho_s c_s$)
π	pi
ρ_s	density of acrylic specimen
v	kinematic viscosity of fluid

have been published [1–11]. These literature reviews had highlighted the paucity of information on jet impingement onto a curved surface.

Only limited papers concerning the jet impingement heat/mass transfer on a curved surface have been identified. Kumada et al. [12,13] investigated the local and mean mass transfer on a cylinder in the potential core and developed (transition) regions of a slot jet. The local Sherwood number distribution due to a slot jet impinging normally on a cylinder differed remarkably from that in uniform flow and was strongly affected by the Coanda effect as a cylinder in shear flow. Potts [14] studied the effects of a round turbulent jet impinging normally on a circular cylinder and the resulting flow field. The relationship between the radius of the nozzle and the cylinder was found to be a vital parameter in the formation of wall jet upon the surface curvature. Sparrow et al. [15] reported that the axial distribution of the heat transfer coefficient peaked at the circular jet impingement point on a cylinder. However, the circumferential distribution of the heat/mass transfer coefficient around the cylinder was not available in their investi-

gation. Gau and Chung [16] studied the surface curvature effects on the different sizes of slot-air-jet impingement cooling flow structure and heat transfer around a concave/convex side of a heated semicylindrical surface. In the convex surface case, it was found that a series of three-dimensional counterrotating vortices around the surface could increase the momentum transport in the flow structure and enhance the heat transfer process on the wall near the stagnation point. The increase of surface curvature could augment the size of the counterrotating vortices, which produced a higher Nusselt number at stagnation point. However, the heat transfer magnitude was reduced in the region away from the stagnation point where the flow became more stable due to the centrifugal force around the surface curvature. Whitaker [17] studied the heat transfer resulting from the impingement of a heated circular jet upon a cylinder. He concluded that the range of nozzle exit temperatures used did not affect much the velocity profiles in the free jet and heat transfer behavior. The flow and heat transfer behavior near the stagnation point region ($S/d<$ 0.2) was independent of target geometry for those impingement distances. Convex target curvature around the circumference of the cylinder enhanced the decay rate of local Nusselt numbers. The transition from a deflection region to a wall jet occurred at 2.5–3 nozzle diameters from stagnation point around the circumference. The Nusselt numbers around the circumference of the cylinder decayed faster than they did along the longitudinal axis.

Recently, Lee et al. [18] have investigated the effects of the hemispherically convex surface curvature on the heat transfer and flow from a fully developed axisymmetric impinging jet. The Nusselt number at the stagnation point, Nu_0 increased with the increasing surface curvature (i.e., increasing value of d/D). However, the effect of surface curvature on the heat transfer was found less in the wall jet region compared to its stagnation point region. The local Nusselt number decreased monotonically from its maximum value, $Nu_{0.}$ In their experimental work, for $Y/d = 2$ and $Re_d = 23{,}000$, and for $Y/d \leqslant 4$ and $Re_d = 50{,}000$, the streamwise Nusselt number distributions were observed with increasing values in the region $1.3 \leqslant r/d \leqslant 1.5$ and reached their secondary maxima at $r/d \cong 2.2$. Choi et al. [19] have studied the fluid flow and heat transfer characteristics of a slot jet impinging on a semi-circular concave surface. They have laid the emphasis on interpreting the heat transfer data in association with the measured mean velocity and velocity fluctuations of impinging and evolving wall jets region along the concave surface, particularly, the occurrence and location of secondary peak. McDaniel and Webb [20] have investigated the effect of slot nozzle configurations (i.e., contoured and sharp-edged jet orifices) on the average impingement heat transfer of circular cylinders.

The aim of this work is to investigate the effects of jet Reynolds number, and dimensionless slot nozzle-to-impingement surface distance on the local and average circumferential heat transfer distributions from a turbulent heated air slot jet impinging on a semi-circular convex surface. The average Nusselt numbers of the present and the published correlated data for the flat surface are also compared. To facilitate the present study, a unique liquid crystal calibration technique for alleviating the viewing angle effect during heat transfer measurements on an oblique/curved surface previously developed by Chan et al. [21], using a true-color image processing system has now been fully implemented. The heat transfer data obtained are also useful to researchers for developing and validating numerical heat transfer models.

2. Experimental apparatus and procedures

2.1. Air slot jet flow system

The experimental air jet flow system is shown schematically in Fig. 1. To ensure high air quality, air from the compressed air line passed through a set of air filtering systems, a refrigerated air dryer, a high precision regulator, an air receiver tank, a heating chamber, a high response solenoid valve, then through a settling chamber and contraction containing a layer of aluminum honeycomb to straighten the flow and turbulence eliminating screens to produce uniform velocity profile of the nozzle outlet. The contraction area ratio was 20:1, giving a reduction in area from 125 mm × 125 mm to 6.25 mm × 125 mm, i.e., the slot nozzle exit area. The cross-sectional dimensions of slot nozzle were 6.25 mm (W) × 125 mm (L), which gave an aspect ratio of 20, without significant end effects. The contraction length was calculated to be 153.24 mm and was curved in such a way as to minimize the growth of boundary layer by Chan [22].

Velocity and temperature stability of the slot jet facility were determined by measuring both data every 5 min over a 4-h period due to the thermal inertia of the heater and downstream jet flow system. The mean jet exit velocity, and turbulence intensity, remained steady to within 2%. The particular jet exit temperature and velocity are stable to within 0.2 °C and 0.3 m/s, respectively, after the jet facility has been warmed up for more than 4 h. The required slot jet temperature was set at the temperature controller and a thermocouple feedback loop was employed to maintain a steady air flow temperature at 40 ± 0.2 °C. The solenoid valve was energized from a DC power supply. The change of digital micromanometer pressure reading was used to identify the start time of the test on the recorded video tape. The time to energize the solenoid valve quoted by the

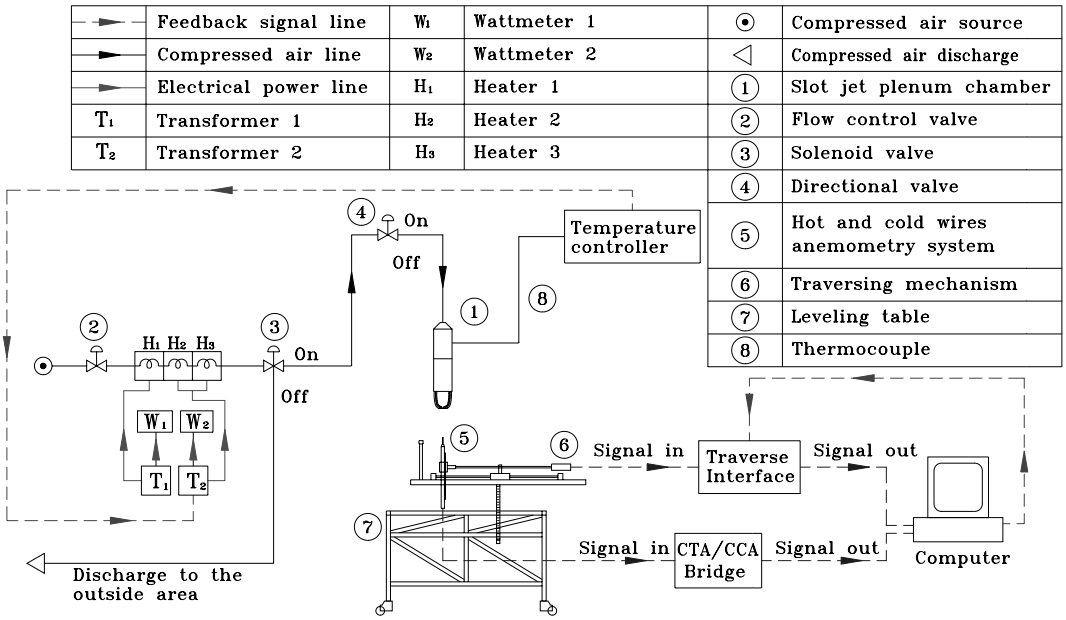

Fig. 1. Schematic diagram of air slot jet flow system.

manufacturer was 32.2 ms which was still less than the 40 ms frame speed of the video camera and the duration of the test. All pipeworks, and the plenum chamber were well insulated to minimize heat losses during the test. The uniformity of the jet exit velocity was monitored using an orifice plate manufactured to BS1042, connected to a digital micromanometer, thus allowing measurement of the differential pressure to within 0.1 Pa. The hot air was then quickly diverted by the solenoid to the exhaust position and the impingement specimen at ambient temperature in the right position (i.e., the slot jet-to-impingement surface distance (Y)). Without further delay, the solenoid valve was re-energized to start the test, and the full field liquid crystal thermographs were recorded on the super-video tape, which obtained a twofold quality of color image compared with the ordinary composite video tape.

A three-wire probe (an X-wire plus a cold wire, the latter placed about 1 mm upstream of the X-wire crossing point and orthogonal to the X-wire plane) was used to measure the velocity and temperature fluctuations in the streamwise and widthwise directions, u and v, respectively. The three-wire probe was traversed across the flow. Similar to [23], the hot wires were etched from a 5 μm diameter Wollaston (Pt–10% Rh) wire to a length of about 1 mm, and a cold wire was etched from a 1.27 μm diameter Wollaston (Pt–10% Rh) wire to a length of about 1.2 mm and a temperature coefficient of 1.69×10^{-3} °C^{-1} was used. Constant-temperature and constant-current circuits were used for the operation of the hot wires and the cold wire, respectively. An overheat ratio of 0.8 was adopted for the X-wire, while a current of 0.1 mA was used in the cold wire. The sensitivity of the cold wire to velocity fluctuations was negligible since the length-to-diameter ratio was about 1000, which is sufficiently large to allow the neglect of any low-wave-number attenuation of the temperature variance. Based on [24], the frequency response of the wire, as indicated by −3 dB frequency, was estimated to be 2.2 kHz at the wind speed investigated. This was sufficient to avoid any high frequency attenuation of the main quantities in the present study. Signals from the circuits were offset, amplified and then digitized using a 16-channel (12 bit) A/D board and a personal computer at a sampling frequency of 3.5 kHz per channel. The duration of each record was about 15 s. The overall uncertainties in the velocity and turbulence were determined to be within 5% and 6%, respectively, based on the suggestion of Browne and Antonia [23]. Details of the validation on the use of a combination of an X-wire and a cold wire anemometery for the present measurements can be found in our previous work in [25,26].

2.2. Heat transfer measurement system

The liquid crystal thermographic system and experimental apparatus are shown in Fig. 2. A semi-cylinder of acrylic, 150 mm diameter, was used as the impingement target surface. In the present study, the calibration plate was prepared at the same time as the semi-circular convex surface test specimen. This is to ensure that the response of thermochromic liquid crystals is consistent by using the same spraying procedures (i.e., black backing paint, the thermochromic liquid crystal ma-

terial, the pressure setting of air artist's brush spraying, the spray distance to the calibration plate and the test specimen, and the number of sprays). A thin layer of 5 °C microencapsulated thermochromic liquid crystal coating was sprayed uniformly onto a water-based soluble black paint surface (Hallcrest, BM/R30C5W/C17-10, R35C5W/C17-10 and BB-G1), which improves the color resolution by absorbing the unreflected light. The total thickness of the combined layers was estimated to be less than 30 μm with a time response within a few milliseconds by Schultz and Jones [27]. Bonnett [28] showed that the thermal conductivity and diffusivity of chiral nematic liquid crystals are similar to those of acrylic material, so the effects due to different thermal resistances have been considered negligible. In addition two thermocouples were placed on the underside of the impingement surface to measure the initial plate temperature (ambient) and validate the semi-infinite assumption.

The CCD video camera was positioned to record the liquid crystal thermographs from a slot jet impingement to the test specimen (a coated liquid crystal and black paint on a semi-cylinder of acrylic). After the tests, the super-video tape was replayed and a color image processing system was used to analyze the recorded color images. Super-video color images can be analyzed at intervals of 40 ms by the PAL color image processing system. The captured color liquid crystal thermographic images can then be used to determine the surface temperature (hence heat transfer information) by the developed transient program with the liquid crystal calibration surface-fit equation. A liquid crystal calibration technique using true-color image processing system in wide-band thermochromic liquid crystals was used to alleviate the effect of video camera viewing angle on a curved surface. Details of liquid crystal calibration facility and procedure are available in [21]. Direct comparisons between surface heat transfer measurements made with transient heating and heated-coating liquid-crystal methods to determine the local heat transfer coefficients on a curved surface can be referred to [29,30]. It is shown that the transient heating liquid crystal method does not require the maintenance of a uniform surface heat flux especially on a larger surface area and therefore there are less limitations on complex model shape (i.e., curved surface), where such

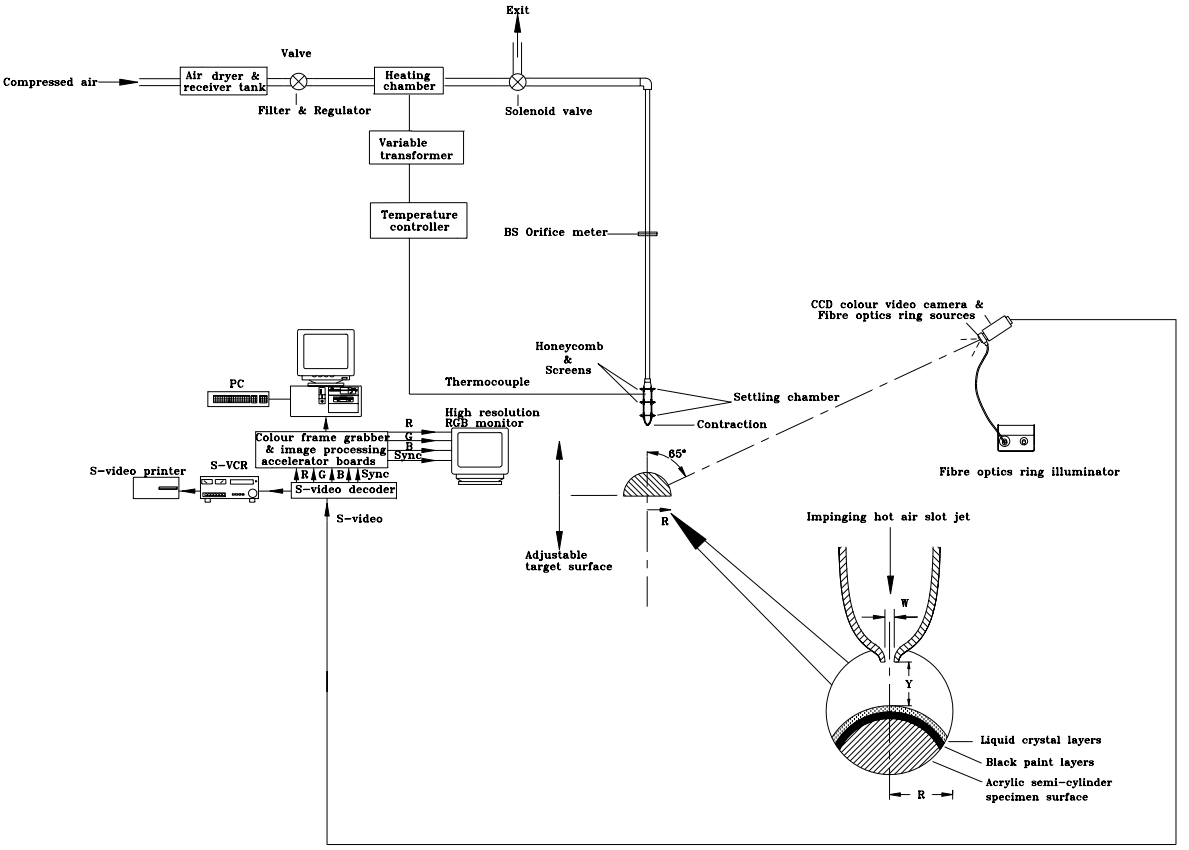

Fig. 2. Experimental set-up for the heat transfer investigation.

non-uniformities are probable. Besides, this transient heating liquid-crystal method has been widely used for very complex geometries, including blade-cooling passages, curved ducts, cylinders, airfoil cooling passages and jet engines [21,31–34].

2.3. Transient heating liquid crystal method

This technique requires measurement of the elapsed time to increase the surface temperature of the liquid crystals coated on test acrylic specimen from a known initial temperature to predetermined value. The rate of heating is recorded by monitoring the color change patterns of the liquid crystal with respect to time. The basic principles and data reduction for transient heating liquid crystal method were described in [31,35]. If the specimen is made from a material with low thermal diffusivity (i.e., acrylic material) and chosen to be sufficiently thick, then the heat transfer process can be considered to be one-dimensional into a semi-infinite medium. Schultz and Jones [27] suggested a criterion for the minimum thickness of material/specimen (s) according to Eq. (1):

$$s > 4\sqrt{\alpha_s t}. \tag{1}$$

The local convective heat transfer coefficient at the surface in the transient method was determined from the response of local surface temperature (liquid crystal color display) to a step change in the fluid temperature, in which one-dimensional heat conduction into a semi-infinite medium was assumed as follows:

$$\frac{T_{(0,t)} - T_{\text{amb}}}{T_{\text{j}} - T_{\text{amb}}} = \phi = 1 - e^{\eta}\left(1 - \text{erf}\sqrt{\eta}\right), \tag{2}$$

where

$$\eta = \frac{h^2 \alpha_s t}{k_s^2}. \tag{3}$$

The partial differentiation of the terms of Eq. (2) and the propagation of the uncertainty in each measured variable through this equation is derived from:

$$\frac{\partial h}{h} = \left[\left(\frac{\delta t}{2t}\right)^2 + \left(\frac{\delta(\sqrt{\rho c_s k_s})}{\sqrt{\rho c_s k_s}}\right)^2 + \left(\frac{1}{\beta(T_{\text{j}} - T_{\text{amb}})}\right)^2 \times \left(\delta T_{(0,t)}^2 + (\phi - 1)^2 \delta T_{\text{amb}}^2 + \phi^2 \delta T_{\text{j}}^2\right)\right]^{0.5}, \tag{4}$$

where

$$\beta = 2\sqrt{\eta}\left[\pi^{-0.5} - \sqrt{\eta}(1 - \phi)\right].$$

The uncertainty in h due to $\delta t/2t$ diminishes as t increases and achieves a maximum for higher values of h. The fractional uncertainty in h due to uncertainty in temperature measurement is a minimum when $\beta(T_{\text{j}} - T_{\text{amb}})$ is large. Detailed uncertainty analysis can be referred to [36]. Chan [30] and Baughn [35] have described that the radiation and conduction corrections with this transient heating liquid crystal technique were small, and these contributions to the overall uncertainty in the heat transfer coefficient were neglected. Hence, the radiation and conduction corrections have not been applied in determining the heat transfer coefficient in the present study. The overall uncertainty in heat transfer coefficient was determined to be within 11% based on individual uncertainties inherent to the experimental arrangement, the alleviation of viewing angle errors on the convex surface, the color image processing system, thermocouple and thermochromic liquid crystal calibration surface-fit equation in [21].

3. Results and discussion

3.1. Slot jet flow characteristics

To characterize the slot nozzle, the axial components of velocities and temperature of free jet were measured along the jet centerline for the jet Reynolds number, Re_W ranging from 5600 to 13,200 for which the corresponding values of slot nozzle exit mean velocity, U_{j} ranging from 15.2 to 35.8 m/s are shown in Figs. 3(a)–(d). Air viscosity and density for Re_W were evaluated at the nozzle exit temperature. The flow could be considered incompressible since the maximum value of nozzle exit velocity did not exceed Mach number of 0.3. Martin [5] stated that the slot jet has a potential core length of approximately 4 slot widths for slot jet, although a wider range from 4 to 7.7 was also found by other investigators [3]. Fig. 3(a) shows that the jet velocity potential core lengths are around 5.7–6.5 slot widths from the centerline nozzle exit velocity $U_{\text{c}} = 0.95\ U_{\text{j}}$ for $Re_W = 5600$, 8500 and 13,200, respectively (i.e., the higher Re_W for the longer potential core length). Figs. 3(b) and (c) show that streamwise Reynolds normal stress reaches its maximum value at earlier Y/W location than that widthwise Reynolds normal stress does. This indicates that streamwise Reynolds normal stress is more sensitive to the expansion of the mixing layer. The jet thermal potential core length decays slightly faster than the jet velocity potential core length because the thermal diffusivity is slightly greater than the momentum diffusivity as shown in Figs. 3(a) and (d). This behavior is in good agreement with the findings from [17,37,38]. It should also be noted that the turbulence intensity increases drastically beyond the potential core region due to more active exchange of momentum with surrounding ambient air, but decays slowly in the fully developed jet region.

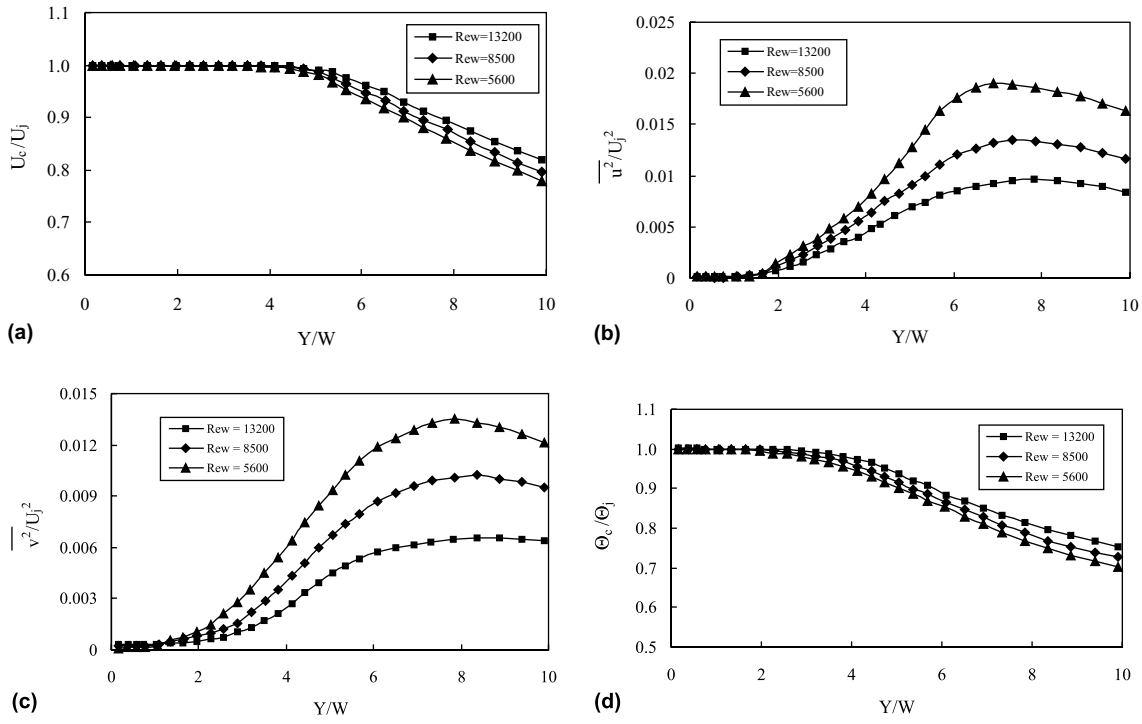

Fig. 3. Normalized (a) mean velocity, (b) streamwise Reynolds normal stress, (c) widthwise Reynolds normal stress and (d) temperature profiles along the free jet centerline at different Re_W.

Only a brief description is given here, the flat velocity profile desired was clearly shown in [22]. With respect to mean axial velocity profiles at the slot nozzle exit, they were flat and uniform to within 3% over approximately the central 90% of the slot nozzle width, and dropping very sharply to almost zero near the nozzle wall. The turbulence intensity profiles across the nozzle width were found to be around 1% intensity in the central region, and rising to about 2% at the nearest location to the nozzle wall. The similar slot configuration jet exit velocity and turbulence intensity profiles were reported in [39].

3.2. Heat transfer results

3.2.1. Liquid crystal calibration surface-fit equations

In order to assess the effect of viewing angle on the temperature versus hue relationship, and to obtain the wide-band thermochromic liquid crystal formulations (e.g., R30C5W and R35C5W) calibration, more than 30,000 raw data of each liquid crystal formulation were recorded and analyzed. Based on a 95% confidence interval, the following generated surface-fit equation (5) correlated to the collected data:

$$T = a + b\exp\left[-0.5\left(\frac{A-c}{e}\right)^2\right] + f\exp\left[-0.5\left(\frac{H-g}{i}\right)^2\right] + j\exp\left[-0.5\left(\left(\frac{A-c}{e}\right)^2+\left(\frac{H-g}{i}\right)^2\right)\right], \quad (5)$$

for the liquid crystal formulation of R30C5W:

$a = 29.6901$, $b = -0.1897$, $c = -95.6411$,

$e = 204.4638$, $f = -0.1985$, $g = 282.3123$,

$i = 113.9105$, $j = 18.3955$,

for the liquid crystal formulation of R35C5W:

$a = 35.9163$, $b = 0.2617$, $c = 126.6718$,

$e = -3.6785$, $f = 22.7094$, $g = 323.6318$,

$i = 99.4188$, $j = 12.5634$,

where T, A and H represent the temperature, viewing/illumination angle from the normal position and hue data, respectively. These generated surface-fit equations

are then used to determine the liquid crystal coated surface temperature of specimen with the transient heating liquid crystal method. Detailed discussion of the color image processing, lighting system, liquid crystal calibration procedure on the effect of viewing/illumination from the normal position can be found in [21,40].

3.2.2. Liquid crystal thermographic images

The applications of liquid crystal thermographic techniques have shown that quantitative as well as qualitative results can be obtained. Some insight into thermal propagation due to a heated air slot jet impinging on a semi-circular convex surface is given by a series of thermal visualization images at various Y/W and $Re_W = 8500$ obtained with a liquid crystal thermographic technique as shown in Fig. 4. Note that only one half of the cylindrical surface is shown due to the symmetric set-up. The symmetry of jet exit velocity and turbulence profiles across the slot nozzle in widthwise direction was in good agreement as evidenced in [22]. The highest temperature (in dark blue/blue contour) was observed at the stagnation region directly beneath the impinging slot jet, and decreasing gradually around the circumferential direction to the lowest temperature (in red contour).

The liquid crystal thermographic images can be captured from a real time or a recorded super-video tape and then processed into useful heat transfer information. The surface heat transfer information was then determined by the transient heating liquid crystal method on the captured liquid crystal thermographic images. All the hue and temperature data for the liquid crystal calibration were captured in real-time frame processing via the digital CCD video camera, super-video cassette recorder, color frame grabber and digital temperature recorder, respectively. The uncertainty in the hue measurement for the captured liquid crystal images was estimated to be less than 1% for the present study as described by Chan [30]. The validation of using

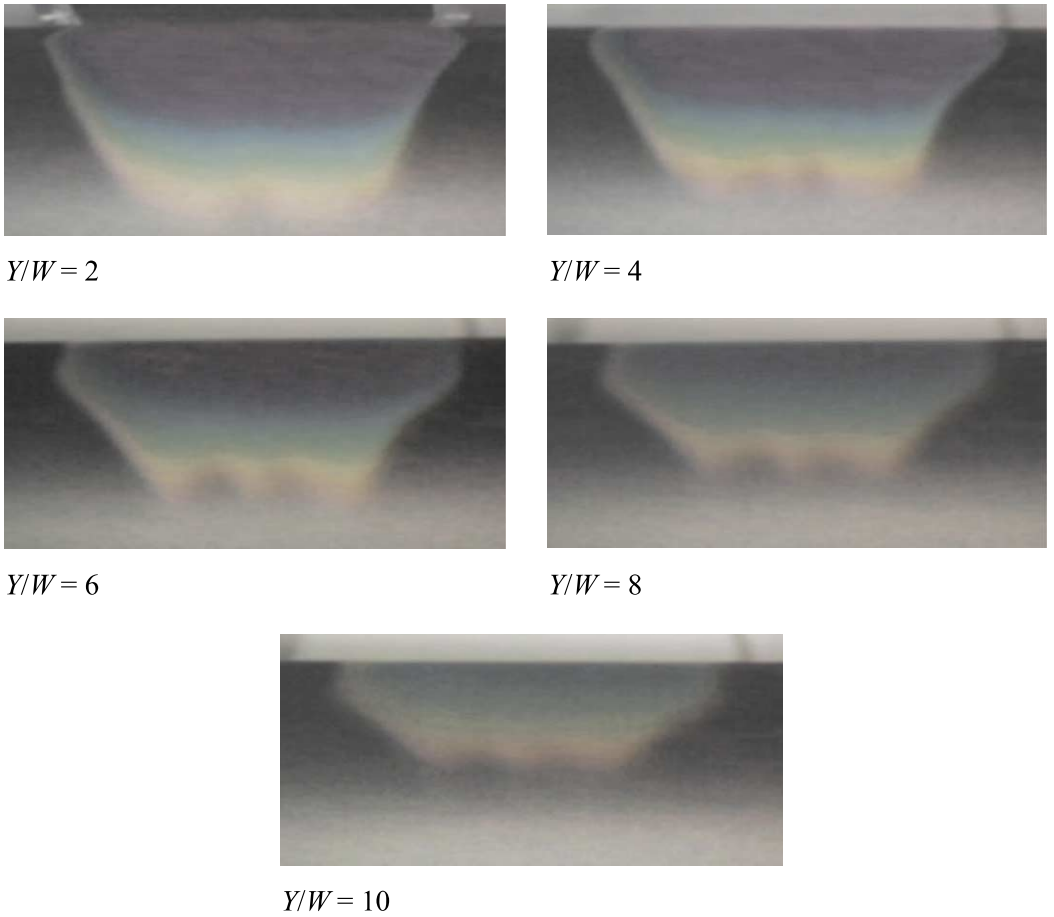

Fig. 4. A typical thermal visualization of a slot jet impinging on a semi-circular convex surface, $Re_W = 8500$.

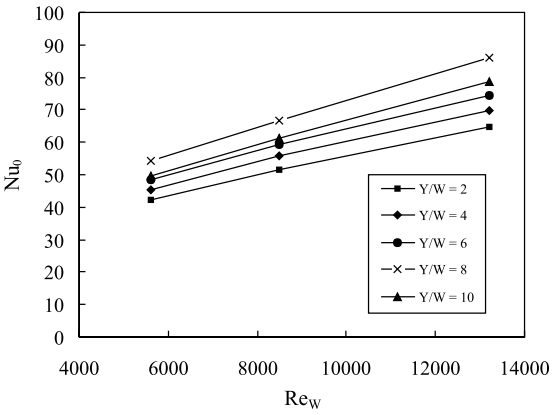

Fig. 5. Effect of jet Reynolds number on the stagnation point Nusselt number.

transient heating liquid crystal method and liquid crystal calibration surface-fit equation for the present heat transfer measurements on a semi-circular convex surface can be found in [21].

3.2.3. Effect of jet Reynolds number

The stagnation point heat transfer is of particular interest for heating, cooling and/or drying purposes because of its relatively high heat transfer rate. The stagnation point Nusselt number (Nu_0) versus the dimensionless slot jet-to-impingement distance (Y/W) at various jet Reynolds numbers (Re_W) is plotted in Fig. 5. The stagnation point Nusselt number increases monotonically for a given jet Reynolds number. All the experiments in the present study were conducted with air and the Prandtl number for air is almost constant over the temperature range used. Correlations of Nu_0 in terms of the Re_W and Y/W are then obtained as follows:

For $2 \leqslant Y/W < 8$

$$Nu_0 = 0.514 Re_W^{0.5} \left(\frac{Y}{W}\right)^{0.124}. \tag{6}$$

For $8 \leqslant Y/W \leqslant 10$

$$Nu_0 = 1.175 Re_W^{0.54} \left(\frac{Y}{W}\right)^{-0.401}. \tag{7}$$

The above correlations are valid for $5600 \leqslant Re_W \leqslant 13{,}200$ with a calculated standard deviation within 1%. Martin [5] and Schlichting [41] have stated that the Nusselt number at the stagnation region should be $Nu_0 \propto Re_W^{0.5}$ for laminar boundary-layer flow for the smaller $Y/W = 2$–6. Fig. 5 shows good agreement with one-half power of jet Reynolds number correlation ($Nu_0 \propto Re_W^{0.5}$). For the longer slot nozzle-to-impingement surface distance of $Y/W > 6$, the jet Reynolds number dependence is stronger ($Nu_0 \propto Re_W^{0.54}$) because these spacings are usually beyond the potential core region and air entrainment effect on the jet momentum takes place. Gardon and Akfirat [42] have discussed in detail the flow phenomena which affect the stagnation heat transfer coefficients. The results agree with the experimental jet Reynolds number correlation at stagnation region from [16,18] for the convex surface case. This information is useful for design purposes if the oblique surface heat transfer rate can be maximized for a single slot impinging jet. The detailed validation of combining this unique calibration technique with the transient heating liquid crystal method by comparing the stagnation Nusselt number of the present data with the relevant published correlated data [16] or experimental data [42] for a similar slot impinging on a convex/flat surface can be found in [21].

Local circumferential Nusselt number distributions (Nu_S) for different jet Reynolds numbers (Re_W) around the semi-circular convex surface are presented in Figs. 6(a)–(c). In each figure, Nu_S is plotted as a function of the dimensionless circumferential distance (S/W), with $S/W = 0$ corresponding to the centerline of the slot impinging jet (or stagnation point). According to these figures, Nu_S increases with increasing Re_W around the convex surface and decreases with increasing the circumferential distance (S) from its maximum value at the stagnation point up to $S/W = 3.1$, where transition in the boundary layer from laminar to turbulent flow occurs and it also causes an increase in the local Nusselt numbers. The transition in the wall jet was completed by about $3.3 \leqslant S/W \leqslant 4.2$ at which secondary peak occurred in this region. But it is noted that the maximum Nu occurred at $S/W \cong 0.21$ from the centerline of the jet for $Y/W \leqslant 4$ for the range of studied jet Reynolds numbers in Figs. 6(a)–(c). A similar slot jet configuration behavior was also found at $Y/W = 4$ from [39]. This occurrence is due to the slot nozzle exit which gives a flat velocity profile indicating that the centerline turbulence level has not reached a fully developed region. The turbulence level in the shear layer at the jet boundary is higher than on the jet centerline. This higher turbulence level causes a small increase in the Nusselt number just adjacent to the centerline of the jet. When the impingement surface is placed beyond the potential core region, the jet flow arriving the impingement is highly turbulent mixing due to the influence of the ambient air entrainment process. The circumferential Nusselt number distributions in a bell shape for $Y/W \geqslant 8$ and the range of studied jet Reynolds numbers are shown in Figs. 6(a)–(c).

Around the circumferential Nusselt number distributions are shown in Figs. 6(a)–(c), the experimental data were correlated as follows:

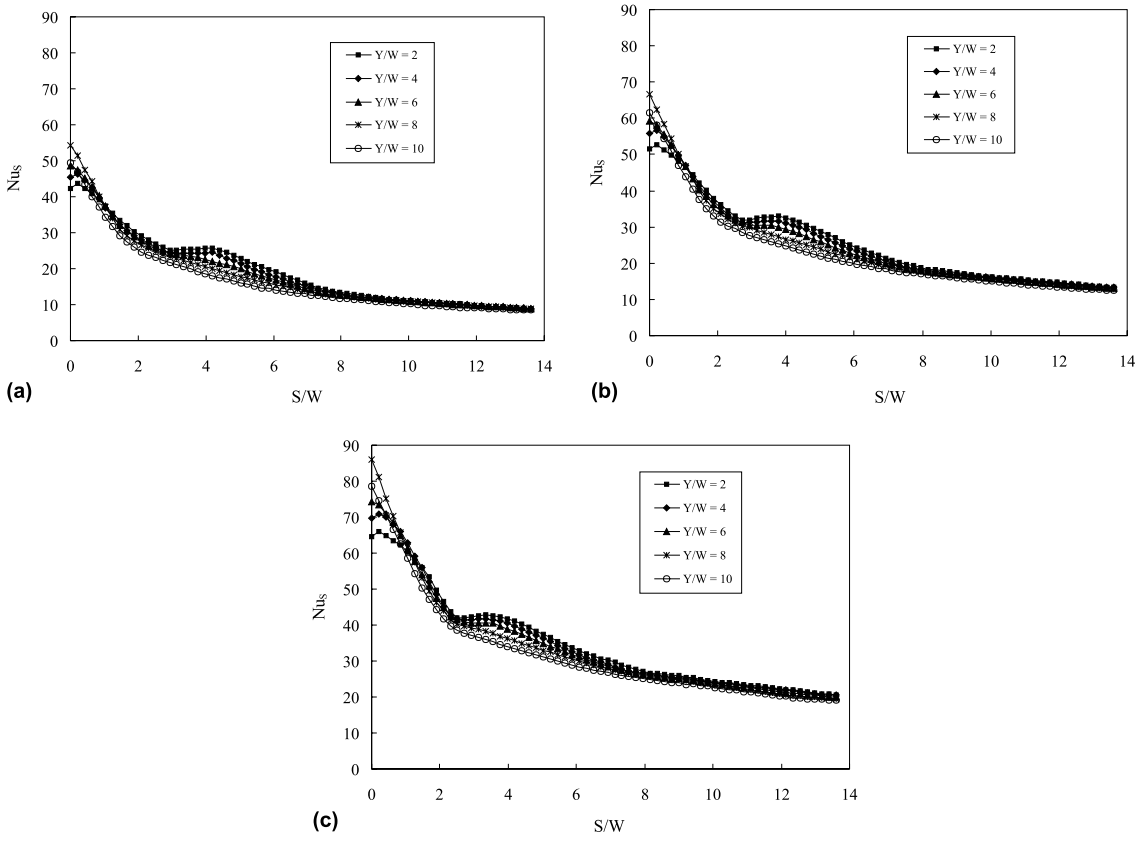

Fig. 6. Circumferential Nusselt number distributions along a semi-circular convex surface at different Y/W and Re_W: (a) $Re_W = 5600$; (b) $Re_W = 8500$, from [21], and (c) $Re_W = 13{,}200$.

For $2 \leqslant Y/W < 8$ and $0 \leqslant S/W \leqslant 13.6$

$$\frac{Nu_S}{Nu_0} = 1.068 - 0.310\left(\frac{S}{W}\right) + 0.079\left(\frac{S}{W}\right)^2 - 0.012\left(\frac{S}{W}\right)^3 + 0.001\left(\frac{S}{W}\right)^4 - 2.141 \times 10^{-5}\left(\frac{S}{W}\right)^5 \quad (8)$$

with a calculated standard deviation of 13.6%.

For $8 \leqslant Y/W \leqslant 10$ and $0 \leqslant S/W \leqslant 13.6$

$$\frac{Nu_S}{Nu_0} = 1.016 - 0.393\left(\frac{S}{W}\right) + 0.1\left(\frac{S}{W}\right)^2 - 0.013\left(\frac{S}{W}\right)^3 + 0.001\left(\frac{S}{W}\right)^4 - 2.089 \times 10^{-5}\left(\frac{S}{W}\right)^5 \quad (9)$$

with a calculated standard deviation of 10.4%.

The above correlations are valid for $5600 \leqslant Re_W \leqslant 13{,}200$.

3.2.4. Effect of the dimensionless slot jet-to-impingement surface distance

It can be seen from Fig. 7 that Nu_0 gradually increases with Y/W and reaches a maximum of $Y/W = 8$.

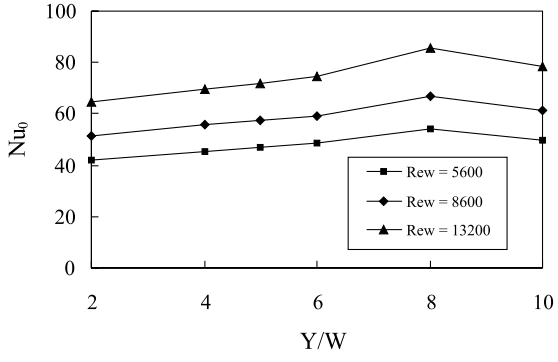

Fig. 7. Effect of slot jet-to-impingement surface separation distance.

A similar non-linear increase Nu_0 behavior for increasing Y/W or Y/d is also found from the previous researchers' work [16,18,42,43]. Figs. 6(a)–(c) correspond to increasing the parameter of dimensionless slot nozzle-to-impingement surface distance (Y/W) from 2 to 10 for three jet Reynolds numbers. In general, the local circumferential Nusselt numbers (Nu_S) decrease from the stagnation point in respect of the parameters of Re_W and Y/W. For $Y/W = 2$ and 4 at low $Re_W = 5600$, the transition starts to take place at $2.9 \leqslant S/W \leqslant 3.2$ and attains secondary peak (turbulent heat transfer) at $S/W \cong 4.2$. For $2 \leqslant Y/W \leqslant 4$ at high $Re_W = 13{,}200$, the transition starts to take place at $2.5 \leqslant S/W \leqslant 2.7$ and reaches the secondary peak at $S/W \cong 3.4$. It is shown that the transition occurs sooner and is completed in a shorter circumferential distance (S) for higher jet Reynolds number. The findings of Cadek and Zerkle [44] and Lee et al. [18] reported similar observation in different target geometries (i.e., flat and convex hemispherical surfaces). Beyond the circumferential distance S/W of about 9 slot width, Nu_S is almost independent of the impingement surface distance with respect to the range of studied jet Reynolds numbers (Re_W). This behavior indicates the existence of a fully developed wall jet at these locations. For $Y/W \geqslant 8$, all figures show that the secondary peak almost disappears due to the stagnation region turbulence effects.

3.2.5. Comparison with the average circumferential Nusselt number distribution on the semi-circular convex surface and flat surface

Becko [4] stated that the average Nusselt number over the local circumferential Nusselt number data is more desirable because such a value is less sensitive to experimental errors and thus more reliable for engineering design. The average circumferential Nusselt numbers are then correlated in terms of Re_W and Y/W over the circumferential distance S/W as follows:

For $2 \leqslant Y/W < 8$ and $0 \leqslant S/W \leqslant 13.6$

$$Nu_{\text{ave}} = 0.514 Re_W^{0.5} \left(\frac{Y}{W}\right)^{0.124} \left[k - \frac{l}{2}\left(\frac{S}{W}\right) + \frac{m}{3}\left(\frac{S}{W}\right)^2 - \frac{n}{4}\left(\frac{S}{W}\right)^3 + \frac{p}{5}\left(\frac{S}{W}\right)^4 - \frac{q}{6}\left(\frac{S}{W}\right)^5\right],$$

where $k = 1.068$, $l = 0.310$, $m = 0.079$,

$n = 1.154 \times 10^{-2}$, $p = 8.133 \times 10^{-4}$,

$q = 2.141 \times 10^{-5}$ (10)

For $8 \leqslant Y/W \leqslant 10$ and $0 \leqslant S/W \leqslant 13.6$

$$Nu_{\text{ave}} = 1.175 Re_W^{0.54} \left(\frac{Y}{W}\right)^{-0.401} \left[k - \frac{l}{2}\left(\frac{S}{W}\right) + \frac{m}{3}\left(\frac{S}{W}\right)^2 - \frac{n}{4}\left(\frac{S}{W}\right)^3 + \frac{p}{5}\left(\frac{S}{W}\right)^4 - \frac{q}{6}\left(\frac{S}{W}\right)^5\right],$$

where $k = 1.016$, $l = 0.393$, $m = 0.1$,

$n = 1.323 \times 10^{-2}$, $p = 8.503 \times 10^{-4}$,

$q = 2.089 \times 10^{-5}$. (11)

The above correlations are valid for $5600 \leqslant Re_W \leqslant 13{,}200$ to be within 14%.

Using the present results, the average circumferential Nusselt number distributions around a semi-circular convex surface were calculated and compared with Martin's flat surface correlation [5], and presented in Figs. 8(a) and (b). These figures show that the average

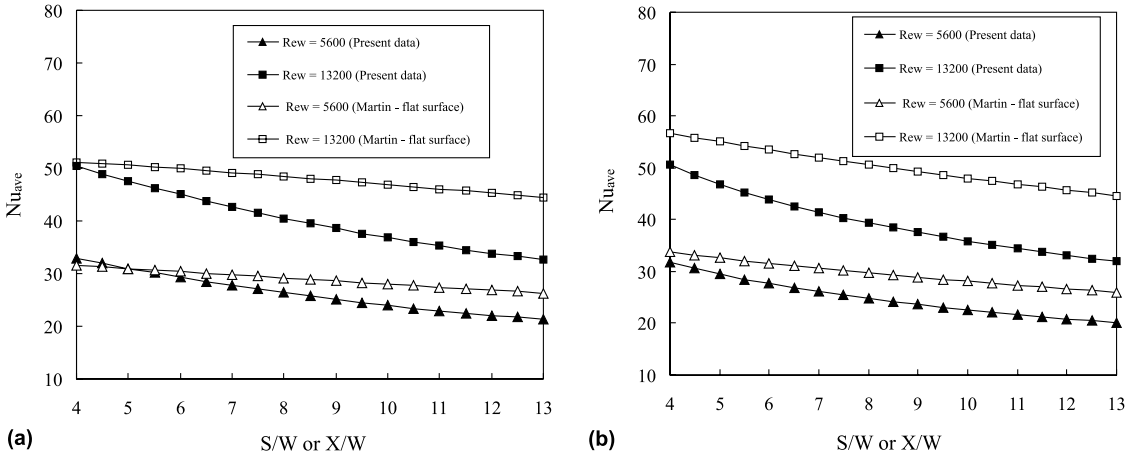

Fig. 8. Comparison of average Nusselt numbers between the present correlated data for a semi-circular convex surface and the published correlated data [5] for the flat surface at (a) $Y/W = 4$ and (b) $Y/W = 8$.

Nusselt numbers increase with increasing jet Reynolds number and decrease with increasing lateral/circumferential distance, Y/W or S/W. The findings of Whitaker [17] tend to support a similar observation. It is also apparent that the decay rate of average circumferential Nusselt numbers around the semi-circular convex surface is much faster than that which occurs laterally along the flat surface. The decrease of Nu_S along the semi-circular convex surface is attributed to the effect of stabilizing the entire flow and reducing the energy and momentum transport near the wall due to the occurrence of a centrifugal force along the surface as described by Schlichting [41] and Mayle et al. [45]. Increasing the circumferential/lateral distance leads to lower the average Nusselt number due to a substantial number of low value local Nusselt numbers occurring in the calculation. It should also be noted that at low slot jet-to-impingement surface distance Y/W (within potential core region), low circumferential distance (i.e., $S/W < 6$) and low turbulent jet Reynolds number, correlations for a flat plate can be used to predict Nu_{ave} to within 5%. This phenomenon is limited to this case. As S/W increases, the effect of curvature becomes apparent and the difference between the flat surface correlation and the present convex surface quickly increases. As Re_W increases, dramatic differences in the curves can be observed, for example at $Re_W = 13{,}200$ and $S/W = 10$, the present correlation leads to about 27% improvement, as shown in Fig. 8(a). As Y/W increases, the difference becomes more pronounced, as shown in Fig. 8(b).

4. Conclusions

An experimental investigation to determine the effects of jet Reynolds number, and dimensionless slot nozzle-to-impingement surface distance on the local and average circumferential heat transfer distributions from a turbulent air impinging slot jet on a semi-circular convex surface has been undertaken. The jet thermal potential core length decays slightly faster than the jet velocity potential core length along the free jet centerline in respect of the jet Reynolds numbers. Nu_0 increases monotonically for the range of studied jet Reynolds numbers and continues to increase non-linearly to its peak values at $Y/W = 8$. The stagnation Nusselt number shows good agreement with $Nu_0 \propto Re_W^{0.5}$ laminar boundary-layer flow for $Y/W = 2$–6 in this study. For the longer $Y/W > 6$, the jet Reynolds number dependence is stronger ($Nu_0 \propto Re_W^{0.54}$) and this is attributed to those distances beyond the potential core region and air entrainment effects on the jet momentum take place.

Nu_S increases with increasing Re_W and decreases with increasing the circumferential distance from its maximum value at stagnation point up to $S/W = 3.1$. The transition in the wall jet from laminar to turbulent flow was completed by about $3.3 \leqslant S/W \leqslant 4.2$ which coincided with a secondary peak which occurred in this region. For $2 \leqslant Y/W \leqslant 4$ at low $Re_W = 5600$, the transition starts to take place at around $2.9 \leqslant S/W \leqslant 3.2$ and reaches a secondary peak (turbulent heat transfer) at $S/W \cong 4.2$. For $2 \leqslant Y/W \leqslant 4$ at high $Re_W = 13{,}200$, the transition starts to take place at around $2.5 \leqslant S/W \leqslant 2.7$ and attains the secondary peak at $S/W \cong 3.4$. It is shown that the transition occurs sooner and is completed in a shorter circumferential distance for higher Re_W. For $Y/W \geqslant 8$, it is shown that the secondary peak almost disappeared due to the stagnation region turbulence effects.

The average Nusselt number around the semi-circular convex surface increases with increasing Re_W and decreases with increasing Y/W or S/W. It is also apparent that the decay rate of average circumferential Nusselt numbers along the semi-circular convex surface is much faster than that which occurs laterally along the flat surface. It should also be noted that at low slot jet-to-impingement distance (within potential core region), low circumferential distance (i.e., $S/W < 6$) and low jet Reynolds number, correlations for a flat plate can be used to predict Nu_{ave} to be within 5%. This phenomenon is limited to this case. As S/W increases, the effect of curvature becomes apparent and the difference between the flat surface correlation and the present convex surface quickly increases. As Re_W increases, dramatic differences in the curves can be observed at $Re_W = 13{,}200$ and $S/W = 10$, the present correlation leads to about 27% improvement when $Y/W = 4$. As Y/W increases, the difference becomes more pronounced.

Acknowledgements

The authors would like to thank The Hong Kong Polytechnic University for the financial support (Project No. A-PB31) towards this work. The first author is particularly thankful to the British Council for their funding which helped to strengthen collaboration between the two universities in the early stages.

References

[1] T.L. Chan, K. Jambunathan, S. Ashforth-Frost, Jet impingement heat transfer – a bibliography: 1870–1977, Previews Heat Mass Transfer 25 (5) (1999) 464–473.
[2] T.L. Chan, K. Jambunathan, S. Ashforth-Frost, Jet impingement heat transfer – a bibliography: 1978–1998, Previews Heat Mass Transfer 25 (6) (1999) 558–570.
[3] J.N.B. Livingood, P. Hrycak, Impingement heat transfer from turbulent air jets to flat plates – a literature survey, NASA TM X-2778, 1973, pp. 1–43.

[4] Y. Becko, Impingement cooling – a review, Von Karman Institute for Fluid Dynamics, Lecture Series 83, January 12–16, 1976, 44 pp.
[5] H. Martin, Heat and mass transfer between impinging gas jets and solid surfaces, Adv. Heat Transfer 13 (1977) 1–60.
[6] P. Hrycak, Heat transfer from impinging jets – a literature review, AFWAL-TR-81-3054, 1981, 63 pp.
[7] S.J. Downs, E.H. James, Jet impingement heat transfer – a literature survey, ASME Paper No. 87-HT-35, 1987, 10 pp.
[8] S. Polat, B. Huang, A.S. Mujumdar, W.J.M. Douglas, Numerical flow and heat transfer under impinging jets: a review, in: C.L. Tien, T.C. Chawla (Eds.), Annual Review of Numerical Fluid Mechanics and Heat Transfer, 1989, vol. 2, pp. 157–197.
[9] B.E. Launder, Turbulence modelling for impinging flows, in: EASE Education and Awareness Programme, ERCOFTAC UK North Pilot Centre and SERC CFD Community Club, Proceedings of the Workshop, UMIST, UK, October 30, 1991.
[10] K. Jambunathan, E. Lai, M.A. Moss, B.L. Button, A review of heat transfer data for single circular jet impingement, Int. J. Heat Fluid Flow 13 (2) (1992) 106–115.
[11] R. Viskanta, Heat transfer to impinging isothermal gas and flame jets, Exp. Thermal Fluid Sci. 6 (1993) 111–134.
[12] M. Kumada, I. Mabuchi, Y. Kawashima, Mass transfer on a cylinder in the potential core region of a two-dimensional jet, Heat Transfer – Jpn. Res. 2 (3) (1973) 53–66.
[13] M. Kumada, I. Mabuchi, Y. Kawashima, M. Hirata, Mass transfer on a cylinder in developed region of a two-dimensional jet, Trans. JSME 30 (330) (1974) 471–478.
[14] D.W. Potts, An experimental study of jet impingement on a circular cylinder, Report No. AFIT/CI/NR 84-50T, 1984, 192 pp.
[15] E.M. Sparrow, C.A.C. Altemani, A. Chaboki, Jet-impingement heat transfer for a circular jet impinging in crossflow on a cylinder, J. Heat Transfer 106 (1984) 570–577.
[16] C. Gau, C.M. Chung, Surface curvature effect on slot-air-jet impingement cooling flow and heat transfer process, J. Heat Transfer 113 (1991) 858–864.
[17] K.W. Whitaker, A study of the heat transfer resulting from a heated jet impinging upon a cylinder, Ph.D. Thesis, Texas A&M University, USA, 1992.
[18] D.H. Lee, Y.S. Chung, D.S. Kim, Turbulent flow and heat transfer measurements on a curved surface with a fully developed round impinging jet, Int. J. Heat Fluid Flow 18 (1997) 160–169.
[19] M. Choi, H.S. Yoo, G. Yang, J.S. Lee, D.K. Sohn, Measurements of impinging jet flow and heat transfer on a semi-circular concave surface, Int. J. Heat Mass Transfer 43 (2000) 1811–1822.
[20] C.S. McDaniel, B.W. Webb, Slot jet impingement heat transfer from circular cylinders, Int. J. Heat Mass Transfer 43 (2000) 1975–1985.
[21] T.L. Chan, S. Ashforth-Frost, K. Jambunathan, Calibrating for viewing angle effect during heat transfer measurement on a curved surface, Int. J. Heat Mass Transfer 44 (12) (2001) 2209–2223.
[22] T.L. Chan, Application of liquid crystal thermography in heat transfer characteristics of slot jet impingement, Ph.D. Thesis, Department of Mechanical and Manufacturing Engineering, The Nottingham Trent University, UK, 1998.
[23] L.W.B. Browne, R.A. Antonia, Reynolds shear stress and heat flux measurements in a cylinder wake, Phys. Fluids 29 (1986) 709–713.
[24] R.A. Antonia, L.W.B. Browne, A.J. Chambers, Determination of time constants of cold wire, Rev. Sci. Instrum. 52 (1981) 1382–1385.
[25] R.A. Antonia, Y. Zhou, M. Matsumura, Special characteristics of momentum and heat transfer in the turbulent wake of a circular cylinder, Exp. Thermal Fluid Sci. 6 (1993) 371–375.
[26] M.H. Liu, T.L. Chan, Y. Zhou, C.W. Leung, A turbulent slot jet impinging on a semi-cylindrical convex surface, in: Proceedings of the 5th International Symposium on Heat Transfer, Beijing, China, August 12–16, 2000, pp. 655–660.
[27] D.L. Schultz, T.V. Jones, Heat transfer measurements in short-duration hypersonic facilities, AGARD 165 (1973).
[28] P. Bonnett, Application of liquid crystals in aerodynamic testing, Ph.D. Thesis, University of Oxford, UK, 1989.
[29] J.W. Baughn, P.T. Ireland, T.V. Jones, N. Saniei, A comparison of the transient and heated-coating methods for the measurement of local heat transfer coefficients on a pin fin, J. Heat Transfer 111 (1989) 877–881.
[30] T.L. Chan, Evaluation of viewing-angle effect on determination of local heat transfer coefficients on a curved surface using transient and heated-coating liquid-crystal methods, Exp. Fluids 31 (4) (2001) 447–456.
[31] P.T Ireland, T.V. Jones, The measurement of local heat transfer coefficients in blade cooling geometries, AGARD Conf. Proc. 390 (Paper 28) (1985).
[32] R.J. Clifford, T.V. Jones, S.T. Dunne, Techniques for obtaining detailed heat transfer coefficient measurements within gas turbine blade and vane cooling passages, ASME Paper No. 83-GT-58, 1983.
[33] H.J. Saabas, S.C. Arora, W.A. Messeh, Application of the transient test technique to measure local heat transfer coefficients associated with augmented airfoil cooling passages, ASME Paper No. 87-GT-212, 1987.
[34] C. Camci, K. Kim, S.A. Hippensteele, P.E. Poinsatte, Evaluation of a hue capturing based transient liquid crystal method for high-resolution mapping of convective heat transfer on curved surfaces, J. Heat Transfer 115 (1993) 311–318.
[35] J.W. Baughn, Review – liquid crystal methods for studying turbulent heat transfer, Int. J. Heat Fluid Flow 16 (1995) 365–375.
[36] S.J. Kline, F.A. McClintock, Describing uncertainties in single-sample experiments, Mech. Eng. 75 (1953) 3–8.
[37] K. Kataoka, T. Takami, Y. Kawachi, Influence of the surrounding fluid on impinging jet, Heat Transfer – Jpn. Res. 6 (3) (1977) 22–35.
[38] S.A. Striegl, The effect of entrainment on jet impingement heat transfer, M.Sc. Thesis, Virginia Polytechnic Institute and State University, USA, 1982.
[39] C. Whitney, Heat transfer characteristics of slot jet impingement, Ph.D. Thesis, Department of Mechanical Engineering, The Nottingham Trent University, Nottingham, UK, 1996.
[40] D.J. Farina, J.M. Hacker, R.J. Moffat, J.K. Eaton, Illuminant invariant calibration of thermochromic liquid crystals, Exp. Thermal Fluid Sci. 9 (1994) 1–12.

[41] H. Schlichting, Boundary Layer Theory, seventh ed., McGraw-Hill, New York, 1979.
[42] R. Gardon, J.C. Akfirat, Heat transfer characteristics of impinging two-dimensional air jets, J. Heat Transfer 88 (C) (1966) 101–108.
[43] Cz.O. Popiel, Th.H. Van der Meer, C.J. Hoogendoorn, Convective heat transfer on a plate in and impinging round hot gas jet of low Reynolds number, Int. J. Heat Mass Transfer 23 (1980) 1055–1068.
[44] F.F. Cadek, R.D. Zerkle, Local heat transfer characteristics of two-dimensional impinging air jets theory and experiment, Heat Transfer 11 (1974) 15–19 (Paper FC1.4).
[45] R.E. Mayle, M.F. Blair, F.C. Kopper, Turbulent boundary layer heat transfer on curved surfaces, J. Heat Transfer (1979) 521–525.